



Chemical processes related to net ozone tendencies in the free troposphere

Heiko Bozem^{1*}, Tim M. Butler², Mark G. Lawrence², Hartwig Harder¹, Monica Martinez¹, Dagmar Kubistin^{1#}, Jos Lelieveld¹ and Horst Fischer¹

5 ¹Max Planck Institute for Chemistry, POB 3060, 55020 Mainz, Germany

²IASS Potsdam, Berliner Strasse 30, 14467 Potsdam, Germany

*now at Johannes-Gutenberg University, Mainz, Germany

#now at DWD, Hohenpeißenberg, Germany

Correspondence to: Heiko Bozem (bozemh@uni-mainz.de)

10 **Abstract.** Ozone (O₃) is an important atmospheric oxidant, a greenhouse gas, and a hazard to human health and agriculture. Here we describe airborne in-situ measurements and model simulations of O₃ and its precursors during tropical and extratropical field campaigns over South America and Europe, respectively. Using the measurements, net ozone formation/destruction tendencies are calculated and compared to 3D chemistry-transport model simulations. In general, observation-based net ozone tendencies are positive in the continental boundary layer and the upper troposphere at altitudes
15 above ~ 6 km in both environments. On the other hand, in the marine boundary layer and the middle troposphere, from the top of the boundary layer to about 6-8 km altitude, net O₃ destruction prevails. The ozone tendencies are controlled by ambient concentrations of nitrogen oxides (NO_x). In regions with net ozone destruction the available NO_x is below the threshold value at which production and destruction of O₃ balance. While threshold NO values increase with altitude, in the upper troposphere NO_x concentrations are generally higher, probably due to the integral effect of convective precursor
20 transport from the boundary layer and NO_x produced by lightning. Two case studies indicate that in fresh convective outflow of electrified thunderstorms net ozone production is enhanced by a factor 5 – 6 compared to the undisturbed upper tropospheric background. The chemistry-transport model MATCH-MPIC generally reproduces the pattern of observation-based net ozone tendencies, but mostly underestimates the magnitude of the net tendency (for both net ozone production and destruction).

25 1 Introduction

Ozone plays a pivotal role in the oxidising capacity of the troposphere. Besides being an oxidising agent itself, photolysis of O₃ at wavelengths less than 340 nm produces O(¹D), whose subsequent reaction with water vapour yields two OH radicals, the dominant oxidant in the troposphere. Based on O₃ profiles in the troposphere, Junge (1963) argued that tropospheric ozone stems from downward transport from the stratosphere and is destroyed at the surface by deposition. But in the 1960s,
30 studies indicated that tropospheric ozone is to a large extent due to in-situ photochemical production, similar to the Los



Angeles smog (Haagen-Smit and Fox, 1956; Leighton, 1961). Budget calculations based on atmospheric chemistry-transport modelling (von Kuhlmann et al., 2003, and references therein) indicate that approximately 390-850 Tg/yr of tropospheric O₃ are due to stratosphere-troposphere-transport, 670-1180 Tg/yr are destroyed by deposition to the surface and -90 to +670 Tg/yr are due to photochemical net ozone production (NOP) in the troposphere (von Kuhlmann et al., 2003, Lelieveld and Dentener, 2000). The NOP itself is a delicate balance between two very large numbers (Lelieveld and Dentener, 2000; von Kuhlmann et al., 2003): ozone production P(O₃) at ~3000-5000 Tg/yr and O₃ destruction L(O₃) at slightly less, ~2500-4500 Tg/yr.

Tropospheric O₃ production is initiated by the oxidation of CO and volatile organic compounds by the OH radical:



The resulting peroxy radicals HO₂, CH₃O₂ and RO₂ subsequently react with NO to produce NO₂:



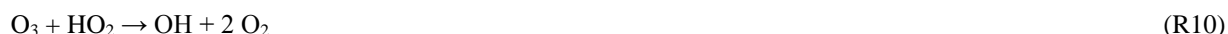
Subsequently, the NO₂ can be photolysed to recycle NO and produce O₃:



In remote regions where VOC concentrations other than CH₄ are low the production of O₃ can be approximated by:

$$P(\text{O}_3) = k(4) [\text{HO}_2] [\text{NO}] + k(5) [\text{CH}_3\text{O}_2] [\text{NO}] \quad (\text{Eq. 1})$$

With k(4) and k(5) being the temperature dependent rate constant of reaction R(4) and R(5). Chemical destruction of O₃ is either due to photolysis or reaction with OH, HO₂ or an alkene:



Whether reaction R8 results in a permanent loss of O₃ depends on the fate of the electronically excited O(¹D) radical. Reaction of O(¹D) with either N₂ or O₂ leads to deactivation and subsequent reformation of O₃, but reaction with water vapour yields two OH radicals, leading to O₃ loss:



The branching ratio among the reactions R12a and R12b mainly depends on the water vapour concentrations and is thus altitude dependent.



In remote regions the reaction with alkenes can be neglected and the ozone loss $L(O_3)$ is given by reactions R8 – R10, with reaction R8 weighted by the branching ratio α :

$$L(O_3) = \alpha JO(^1D) [O_3] + k(9) [OH][O_3] + k(10) [HO_2][O_3] \quad (\text{Eq. 2})$$

Where $JO(^1D)$ is the O_3 photolysis rate and α is given by Eq. 3:

$$\alpha = \frac{k(12a)[H_2O]}{k(12a)[H_2O] + k(12b)[O_2] + k(12c)[N_2]} \quad (\text{Eq. 3})$$

The branching ratio α is typically of the order of 1 to 15 % for the upper troposphere and the boundary layer, respectively. Note that we also neglect loss of NO_2 due to reaction with OH, yielding nitric acid, and we do not account for the production of peroxy nitrates. This is justified by the overall low NO_x concentrations outside the continental boundary layer.

10 The net ozone production rate (NOPR) in ppbv/h is defined as the difference between production and loss:

$$NOPR = P(O_3) - L(O_3) \quad (\text{Eq. 4})$$

Net photochemical ozone production in the troposphere is a non-linear function of the concentration of the peroxy radicals produced in reactions R4 – R6, and their precursors, as well as the concentration of NO. The threshold NO concentration (NO_{th}) at which the production $P(O_3)$ equals the loss $L(O_3)$ depends on the relative strength of reaction R4 to reaction R10, which both compete for the HO_2 radical. With reaction R4 being approximately 4000 times faster than R10 a typical range for NO_{th} is 10-20 pptv at an ozone concentration of about 50 ppbv. Below this NO_{th} concentration O_3 destruction prevails, while net production occurs at higher NO concentrations.

Model studies indicate that chemical O_3 destruction is generally found in the lower troposphere over the oceans due to low NO and high H_2O concentrations, while generally higher NO_x concentrations in the continental boundary layer lead to net O_3 production (Klonecki and Levy, 1997). Over the oceans O_3 loss extends to the free troposphere, while enhanced NO_x due to lightning or convective up-lift of NO_x from anthropogenic or biomass burning sources leads to O_3 production above the continental boundary layer (Roelofs and Lelieveld, 1997). This difference between oceanic and continental free troposphere vanishes in the upper troposphere, where O_3 production prevails (Klonecki and Levy, 1997; von Kuhlmann et al., 2003). Studies that infer net ozone production at least in part from in-situ measurements are rare and often limited to the boundary layer (Ren et al., 2013; Liu et al., 2012; Sommariva et al., 2011; Kuhn et al., 2010; Kleinman, 2005; Kondo et al., 2004; Cantrell et al., 2003a; Cantrell et al., 2003b; DiNunno et al., 2003; Ko et al., 2003; Fischer et al., 2003; Reeves et al., 2002; Kanaya et al., 2002; Kleinman, 2000; Zanis et al., 2000; Penkett et al., 1997; Cantrell et al., 1996). Carzola and Brune (2010) described the application of an in-situ instrument to measure ozone production, while estimating the NOP requires in-situ measurements of radicals (OH, HO_2 , RO_2), nitrogen oxide (NO) and photolysis rates (i.e. $JO(^1D)$) in addition to ozone and water vapour. Here we present airborne in-situ measurements of radicals and ozone precursors over the tropical rainforest in South-America during the GABRIEL (Guyanas Atmosphere-Biosphere exchange and Radicals Intensive Experiment with a Learjet) campaign in October 2005, and compare with a series of north-south transects over Europe in the extratropical troposphere as part of the HOOVER (HOx OVer EuRope) campaign in 2006 and 2007.



2 Methods

2.1 GABRIEL and HOOVER measurements

The GABRIEL campaign took place in October 2005 over the tropical rainforest in French Guyana and Surinam. A total of
5 10 measurement flights, each between 3 and 3.5 hours long, were performed between 3° and 6°N and 59° to 51°W at
altitudes between 300 and 9000 m (Figure 1a). All flights followed a similar pattern, with take-off from Zanderij airport
(Surinam, 5.3°N, 55.1°W), followed by a high altitude stretch east over the Atlantic Ocean, and a descent into the marine
boundary layer off the east coast of South America. Turning west the aircraft followed the main wind direction in-land,
performing flights in and out of the continental boundary layer over the rainforest. Finally, before landing at the home base a
10 high altitude profile was flown over Surinam. Additionally, similar flight profiles were performed in the N-S direction. Take-
off times of the flights were varied over the campaign in order to investigate diurnal variations. Details of the scientific
objectives, measurement and model results can be found in Lelieveld et al. (2008) and the GABRIEL special issue in
Atmospheric Chemistry and Physics (http://www.atmos-chem-phys.net/special_issue88.html).

HOOVER consisted of a total of two measurement campaigns in October 2006 and July 2007, composed of 4 measurement
15 flights each. The measurements covered Europe from 40° to 75°N between 8° and 15°E and up to a maximum altitude of 12
km (Figure 1b). From the home base Hohn (Germany, 54.2°N, 9.3°E) regular research flights were performed southward
with a stop-over at Bastia airport, Corsica (France, 42.2°N, 9.29°E) and northward with a stop-over at Kiruna airport
(Sweden, 67.5°N, 20.2°E). The majority of the flights were performed in the upper troposphere, but regular profiles were
flown in and out of the home and stop-over bases, as well as approximately half way towards the respective destination in
20 either Southern Germany or Northern Scandinavia. Additional flights in summer 2007 were directed to the Arctic (Svalbard,
Norway, 78.1°N, 15.3°E) and two flights over central Germany to study the influence of deep convection. Details about the
campaigns can be found in two previous publications (Klippel et al., 2011; Regelin et al., 2013).

2.2 Observations

25 During both campaigns a Learjet 35A from GFD (Hohn, Germany) was used. This jet aircraft has a range of 4070 km and a
maximum flight altitude of approximately 14 km. In the present configuration both the horizontal and vertical range were
limited due to the use of two wing-pods housing additional instrumentation. The scientific instrumentation was similar
during both campaigns. It consisted of a chemiluminescence detector (ECO Physics CLD 790 SR, Switzerland) for NO, NO₂
and O₃ measurements (Hosaynali Beygi et al., 2011), a set of up- and downward looking 2π-steradian filter radiometers for
30 J(NO₂) measurements (Meteorologie Consult GmbH, Germany), a quantum cascade laser IR-absorption spectrometer for
CO, CH₄ and HCHO measurements (Schiller et al., 2008), a dual enzyme fluorescence monitor (model AL2001 CA peroxide



monitor, Aerolaser, Germany) to measure H_2O_2 and organic hydroperoxides (Klippel et al., 2011), a laser induced fluorescence (LIF) instrument for simultaneous measurements of OH and HO_2 (Martinez et al., 2010; Regelin et al., 2013), a non-dispersive IR-absorption instrument (model LI-6262, Li-COR Inc., USA) for CO_2 and H_2O measurements (Gurk et al., 2008), a proton transfer reaction mass spectrometer (PTR-MS, Ionicon, Austria) for partially oxidized volatile organic compounds measurements and a series of canisters for post flight analysis of non-methane hydrocarbons (Colomb et al., 2006). Here a sub-set (O_3 , NO, CO, CH_4 , H_2O , OH, HO_2 and $\text{J}(\text{NO}_2)$) of these measurements will be used to deduce NOPR values. Details about the performance of those measurements with respect to time resolution, precision, detection limits and total uncertainties can be found in Table 1.

10 2.3 Estimating peroxy radical concentrations and $\text{J}(\text{O}^1\text{D})$

Most species that are needed for an evaluation of equations 1 – 4 are provided by in-situ observations with the exception of $[\text{CH}_3\text{O}_2]$ in Eq. 1 and $\text{J}(\text{O}^1\text{D})$ in Eq. 2, that have to be derived from other measurements.

As mentioned in the introduction, we assume that in remote areas outside of the continental boundary layer, the concentrations of other volatile organic compounds besides methane are low, so that CH_3O_2 is the only organic peroxy radical at significant concentrations in view of O_3 formation. According to R1 and R2 the production rates for HO_2 and CH_3O_2 radicals are proportional to the concentrations of CO and CH_4 , respectively. Since the photochemical lifetimes of both radicals with respect to their reaction with NO (R4, R5) or self-reactions leading to peroxides are similar (Hosaynali Beygi et al., 2011; Klippel et al., 2011), we assume that the ratio of $\text{HO}_2/\text{CH}_3\text{O}_2$ is proportional to their production rates $k_{(\text{CO} + \text{OH})}[\text{CO}][\text{OH}]/k_{(\text{CH}_4 + \text{OH})}[\text{CH}_4][\text{OH}]$, so that the concentration of CH_3O_2 can be deduced from equation 5:

$$20 \quad [\text{CH}_3\text{O}_2] = \frac{k(2)[\text{CH}_4]}{k(1)[\text{CO}]} [\text{HO}_2] \quad (\text{Eq. 5})$$

Thus using measured mixing ratios for CO, CH_4 and HO_2 and the temperature dependent rate coefficients for R1 and R2, the mixing ratio of CH_3O_2 can be estimated. Hosaynali Beygi et al. (2011) have used this approach in the marine boundary layer and compared it to both box model and 3D chemical transport model simulations in order to demonstrate the applicability of Eq. 5 in remote regions. We expect this to also hold for the free troposphere. In the continental boundary layer and in the outflow of deep convective clouds, R4 will most probably underestimate peroxy radical concentrations and thus O_3 production according to Eq. 1.

The O_3 photolysis rate $\text{J}(\text{O}^1\text{D})$ and $\text{J}(\text{NO}_2)$ were calculated with the radiation transfer model TUV (<https://www2.acom.ucar.edu/modeling/tropospheric-ultraviolet-and-visible-tuv-radiation-model>) (Madronich and Flocke, 1999) and scaled to the observed $\text{J}(\text{NO}_2)$ values.

30



2.4 MATCH simulations

To compare the experimentally derived NOPR values with model simulations the 3D chemistry transport model MATCH-MPIC (Lawrence et al., 2003; von Kuhlmann et al., 2003) (hereinafter referred to simply as MATCH) has been used. The model is driven by meteorological data from the National Centre for Environmental Prediction (NCEP) Global Forecast System (GFS). The chemical scheme, including details of the non-methane hydrocarbon chemistry, is described in von Kuhlmann et al. (2003). The model was run with a resolution of approximately $2.8^\circ \times 2.8^\circ$ in the horizontal direction and includes 42 vertical σ -levels up to 2 hPa. Emissions from anthropogenic and natural sources are based on the Emission Database for Global Atmospheric Research EDGAR v3.2 (Olivier et al., 2002). The model has been used for chemical weather forecasting to guide the day-to-day flight planning during GABRIEL and HOOVER. Here we used post-campaign analysis simulations to produce virtual flights through the model along the actual aircraft trajectories, as done in Fischer et al. (2006). From the model results NOPR values derived from a full chemistry scheme including also higher order peroxy radicals have been calculated for every point along the flight tracks.

3 Results

3.1 Data Processing

In the following, net ozone production rates in ppbv/h are calculated from in-situ data according to Eq. 4, with ozone production $P(\text{O}_3)$ calculated from Eq. 1, including Eq. 5 for $[\text{CH}_3\text{O}_2]$ and ozone loss $L(\text{O}_3)$ from Eq. 2 with Eq. 3 for α . A filter ($\text{O}_3 < 100$ ppbv) was applied to the data to exclude direct stratospheric influence. Data from two flights dedicated to the investigation of deep convection (GABRIEL flight GAB 08 on 12 October 2005 (Bozem et al., 2014) and HOOVER II flight 07 on 19 July 2007) were not included, and will be discussed separately. For the remaining data tropospheric NOP rates were calculated along the flight tracks using merged data sets with a time resolution of 30 s. Instead of presenting the NOP data as a time series for individual flights, we make use of the sampling strategy followed in the two campaigns. As can be seen in Figure 1, flights during Gabriel were mostly oriented from east to west (in Fig. 1a), while flights during HOOVER had a north south orientation (Fig. 1b). Therefore, all NOP data from the individual flights have been binned into altitude-longitude (GABRIEL) and altitude-latitude (HOOVER) bins. The bin size is 1 km in altitude, 0.5° in longitude (GABRIEL) and 2.5° in latitude (HOOVER). NOP values are presented as median values for a given altitude/longitude (GABRIEL) or altitude/latitude (HOOVER) bin. Additionally, the 1σ -standard deviation of the individual NOP values in the respective bin is given as a measure of the atmospheric variability. Since NOP values can only be calculated for those bins that have at least one data point for each trace gas species needed in Eq. 1 – 5 (O_3 , NO, CO, CH_4 , H_2O , OH, HO_2 and $\text{J}(\text{NO}_2)$), missing data due to instrument failures strongly limit data coverage. This is a severe limitation for GABRIEL in particular due to missing CO and H_2O values on some flights and missing NO values due to an instrument failure during the HOOVER II south-bound flights in summer 2007. To overcome this, average altitude profiles for CH_3O_2 and H_2O have been calculated for the



GABRIEL data set to substitute missing values by median values from the profiles for a particular altitude bin. Data gaps due to missing values in other species were replaced in a similar way by median values from the mean altitude profiles. This way the available number of NOPR calculations could be increased by a factor of 4, without changing trends in NOPR for different regions. Similar data gaps during HOOVER I and II have been handled accordingly. Further, for HOOVER II, NO data are not available from the flights to and from Corsica, thus in particular south of the Alps NOPR calculations cannot be based on in-situ data. Based on an additional flight between the home base in Northern Germany and Northern Italy (HOOVER II flight 06 from Hohn to Baaden Airport (Germany) on 19 July 2007), an average NO profile has been calculated for the southern part of Europe and used as a proxy for missing NO values. Note that data from HOOVER II flight 07 on the same day have not been used, since they were affected by strong convection over south-eastern Germany. Uncertainties due to the missing NO data during HOOVER II will be discussed further below.

Simulation results for $P(O_3)$, $L(O_3)$ and NOPR along the flight trajectories obtained from MATCH have been filtered for stratospheric influence, processed and binned in a similar way as the in-situ data and will be presented together with the in-situ data.

3.2 NOPR for GABRIEL

Figure 2 shows results for NOPR calculations based on in-situ measurements (Fig. 2a) and MATCH simulations (Fig. 2b) for the GABRIEL campaign in October 2005. As mentioned above NOPR values have been calculated along the flight tracks and sampled into bins of 1 km height and 0.5° longitude. The median values of NOPR per bin are presented with different colours, ranging from blue (negative NOPR indicating net O_3 destruction) to red (positive NOPR indicating net O_3 production). The number of data points within a bin is given as a number in the lower left corner. The circle inside the bin is a measure of the variability, with a box filling circle indicating a variability of more than 50 % relative to the median. Note that a variability value is presented even if only 2 data points are available for an individual bin. Both figures are oriented from west to east, so that data over the Atlantic Ocean are on the right hand side of the figure. With the South American coastline located between $53.5^\circ W$ and $53.0^\circ W$, bins east of this longitude are representative for marine air masses and bins towards the west represent continental air masses.

In the lowest bins (0 – 1 km altitude) representing the boundary layer, NOPR values indicate a change from O_3 destruction in the marine boundary layer (-0.2 to -0.4 ppbv/h between $51^\circ W$ and $54^\circ W$) towards a highly variable O_3 production (0 – 0.6 ppbv/h) regime in the continental boundary layer over the tropical rainforest ($54^\circ W$ to $57.5^\circ W$) (Fig. 2a). Highest NOPR values are observed at the coast at $52.5^\circ W$ – $53^\circ W$, probably due to local pollution in the vicinity of Cayenne, the capital of French Guyana. Note that the absolute values for NOPR in the boundary layer, in particular over land, are less reliable, since we do not consider the contributions of higher organic peroxy radicals to ozone production and also neglect an additional O_3 sink due to reaction with alkenes, in particular isoprene. In the free troposphere, above 1 km and below 6 km altitude, NOPR values are generally negative, with strongest O_3 destruction in the first 2 km above the boundary layer. Above 6 km there is



again a region with slightly positive NOPR, hence net O₃ production. In general, above the boundary layer NOPR values exhibit no difference between marine and continental regions. Note that similar results are obtained from calculations based only on the sub-set of data points for which simultaneous in-situ measurements of all species necessary to calculate NOPR are available. Thus, replacing the missing values by median values from average profiles does not change the results significantly. This statement holds also for results from the other campaigns, with the exception of missing NO measurements south of 55°N during HOOVER II. This will be addressed in section 2.4.

The MATCH simulations (Fig. 2b) exhibit similar NOPR tendencies for the different altitude regimes, though the absolute values are generally smaller (-0.2 ppbv/h and 0.1 ppbv/h, respectively). Also, MATCH simulates net O₃ destruction in the continental boundary layer over the tropical rainforest, in contrast to the calculation derived from the in-situ observations (Fig. 2a).

Net ozone production is expected to be strongly dependent on the NO concentration. The threshold NO concentration, at which ozone production and loss are equal, can be calculated by setting

$$P(\text{O}_3) = L(\text{O}_3) \quad (\text{Eq. 6})$$

and re-arranging for NO:

$$NO_{th} = \frac{\alpha[(\text{O}^1\text{D})[\text{O}_3] + k(10)[\text{HO}_2][\text{O}_3] + k(9)[\text{OH}][\text{O}_3]}{k(4)[\text{HO}_2] + k(5)[\text{CH}_3\text{O}_2]} \quad (\text{Eq. 7})$$

In Figure 3 the ratio between NO and NO_{th} is plotted for in-situ data (Fig. 3a) and MATCH simulations (Fig. 3b). According to Eq. 7 the measurement-calculated threshold NO concentration in the boundary layer is 9 pptv, while it increases to about 20 pptv above the boundary layer. This is mainly due to the decrease of observed HO₂ and estimated CH₃O₂ concentrations above the boundary layer, which leads to an increase of the threshold NO value. Measured NO mixing ratios are higher than the threshold values in the continental boundary layer (approx. 2 times larger), and at altitudes above 6 km (up to 3 times larger) (Fig. 3a), indicating net ozone production regimes as shown by Fig. 2a.

The evaluation of MATCH shows a slightly different altitude-dependent behaviour of NO_{th}, with highest values (21 pptv) in the boundary layer, decreasing almost linearly with altitude to lowest values of 10 pptv at 8 km. Figure 3b shows that simulated NO concentrations in MATCH are almost always lower than the threshold values (NO/NO_{th} ratio between 0 and 1), except at the highest altitudes (NO about 50% higher than NO_{th}), thus explaining the overall negative NOPR values in Fig 2b. Therefore, the deviations between model simulations and in-situ data for NOPR are due to differences in the threshold NO levels (NO_{th}) and generally lower NO concentrations in the model simulations. Discrepancies in NO_{th} by the MATCH model are possibly related to the non-methane hydrocarbon chemistry scheme, which may underestimate radical recycling under low NO_x conditions and high isoprene (Kubistin et al., 2010; Taraborrelli et al., 2012).

In general, the charts of the NO to NO_{th} ratio resemble the NOPR charts, with ratios larger than unity corresponding to net ozone production and ratios less than unity to ozone destruction. The values also scale quantitatively, illustrating the strong dependency of NOPR on NO mixing ratios. At the rather moderate NO levels in the free troposphere this relationship seems to be linear. This behaviour is also found in the data from the other campaigns.



3.3 NOPR for HOOVER I

Figure 4 shows results for NOPR calculations based on in-situ (Fig. 4a) and MATCH simulations (Fig. 4b) for the HOOVER I campaign in October 2006 over Europe. For this campaign the data for NOPR have been combined into 1 km altitude and 2.5° latitude bins. The majority of the data is obtained in the upper troposphere, while vertical profiles are restricted to take-offs and landings in airports on Corsica (40° - 42.5° N), Hohn (52.5° - 55°N) and Kiruna (67.5° - 70°N). Additional profiles were flown north and south of the Alps (45° - 50°N) and over Sweden (60° - 62.5°N). Overall, the in-situ data indicate net ozone production (0.1 - 0.3 ppbv/h) throughout the troposphere, except at the most northern (0 ppbv/h) and southern (~ -0.1 ppbv/h) parts of the flights. Threshold NO values are between 15 and 20 pptv up to 10 km altitude, above which they linearly increase to approx. 35 pptv at 12 km. In regions with net ozone production (NOPR > 0 ppbv/h), measured NO concentrations are up to a factor of 4 higher than NO_{th}. In the regions with NOPR ≤ 0 ppbv/h the measured NO concentration is smaller than NO_{th} (not shown).

MATCH simulations of NOPR (Fig. 4b) exhibit slightly lower values (0 - 0.1 ppbv/h) compared to those derived from in-situ data, but the general tendencies are reproduced well. The only exception is the vertical profile over Sweden, where the observations indicate strong ozone production due to high NO concentrations, which are not reproduced by MATCH. Overall, MATCH tends to underestimate NO concentrations throughout the troposphere, possibly related to underestimated vertical mixing of pollution from the boundary layer or missing NO_x reservoir species such as alkyl nitrates in the chemistry scheme.

20

3.4 NOPR for HOOVER II

As mentioned above, NOPR calculations for HOOVER II are strongly affected by the failure of the CLD instrument used for NO measurements on the flights to the south, from Hohn to Corsica and back. Figure 5a shows results for NOPR calculations based on this limited data set. The NOPR calculations based on in-situ data are limited to latitudes north of 50°N. At higher latitudes a similar pattern to that during HOOVER I is observed, with net ozone production in the boundary layer, negligible to negative NOPR in the middle troposphere and a tendency for moderate net ozone production in the upper troposphere. This general pattern is reproduced by MATCH simulations north of 50°N as shown in Fig. 5d.

In order to improve the data coverage, in particular south of 50°N, we used an average NO profile measured on 19 July 2007. On this day, two measurement flights were performed (HOOVER II flights 06 and 07), to study deep convection over Southern Germany out of Baaden airport (48.4°N, 8.4°E). Since no nitric oxide measurements were obtained on the regular flights south, the transfer flight to Baaden airport was extended southward to Northern Italy. Thus a limited data set of NO could be obtained south of 50°N. Profile information is available from a descent north of the Alps close to Oberpfaffenhofen

30



(48.4°N, 11.1°E) and the landing at Baden airport. From this data set an average profile was deduced and median values have been used in the calculation of NOPR south of 55°N (Fig. 5b). This led to overall negative ozone tendencies throughout the troposphere at latitudes south of 50°N in contrast to the MATCH simulations that predict net ozone production (Fig. 5d). Both the model and NO_{th} calculations based on in-situ data indicate a threshold NO concentration of 15 – 20 pptv between
5 the boundary layer and approx. 9 km altitude (with strongly increasing NO_{th} above this altitude), with the model calculating slightly smaller values. The MATCH model simulates NO concentrations south of 55°N that are a factor of 2 to 3 higher than the simulated NO_{th} . The NO values from the HOOVER II flight 06 profile used to fill in data gaps south of 50°N are more than 50 % lower than the deduced NO_{th} based on in-situ observations. Thus the negative ozone tendencies in Fig. 5b are mainly due to an underestimation of NO mixing ratios. Therefore, a sensitivity study was performed by doubling the NO
10 concentrations obtained from the HOOVER II flight 06 profile. The results for NOPR are shown in Figure 5c. The doubling of NO mixing ratios leads to a shift to positive NOPRs south of 55°N and to a much better agreement with the model simulations shown in Fig. 5d. It should be mentioned that the enhanced NO mixing ratios are in rather good agreement with NO measurements obtained over southern Germany and northern Italy in the summer of 2003 as part of the UTOPIAN-
ACT campaign (Stickler et al., 2006). Thus it seems that the NO mixing ratios from the HOOVER II flight 06 profile may
15 not be representative of background NO south of 50°N.

Overall, a general feature of the three missions is a tendency of net ozone production at the highest altitudes, although we calculate strong increases of NO_{th} with altitude. For HOOVER II both model simulations and observation-based calculations indicate a doubling of NO_{th} between 9 and 11 km altitude from approx. 20 pptv to more than 40 pptv. As mentioned in the previous sections, similar tendencies for NO_{th} were also deduced for HOOVER I and GABRIEL. In order to maintain
20 positive NOPR at high altitudes a strong enhancement of NO above 10 km is required. In the next section we will discuss the influence of deep convection on NOPR based on two case studies during GABRIEL and HOOVER II, respectively.

3.5 The influence of deep convection on NOPR

As outlined in section 2.1 the analysis thus far has been restricted to “background conditions” by filtering data that have been
25 affected by deep convection. Research flights to study the outflow of deep convection have been performed during both GABRIEL (Bozem et al., 2014) and HOOVER II (Regelin et al., 2013). Details about the convective systems, the flight tracks and trace gas measurements can be found in these articles.

During GABRIEL the outflow of a single convective cell at 9 to 11 km showed enhancements relative to background mixing ratios for CO, NO, OH and HO_2 of 40%, 130%, 70% and 20%, respectively. The CO increase with altitude suggests a strong
30 contribution of boundary layer air. Transport of HO_x precursors from lower layers of the troposphere led to enhanced OH and HO_2 concentrations in the outflow. The strong enhancement in NO is most likely due to additional NO production from lightning. Ozone mixing ratios were also enhanced (38%), which may contradict the expectation that transport of boundary layer air in convective systems should lead to a decrease of O_3 mixing ratios in the outflow relative to the undisturbed middle



and upper troposphere. A detailed discussion of the trace gas budgets, in particular for O₃, can be found in Bozem et al. (2014). Figure 6a shows mean and median values for NOPR in the outflow at the 10.5 km bin relative to campaign background median and mean altitude profiles for non-convective air masses. The median value of 0.2 ppbv/h (mean: 0.27 ± 0.13 ppbv/h) is roughly a factor of 3 higher than the background value (median: 0.06 ppbv/h; mean: 0.06 ± 0.04 ppbv/h).

5 This is mainly due to the enhancement of NO, in addition to the increase of peroxy radical concentrations.

In order to compare the GABRIEL results for NOPR with literature data for the tropics we estimate daily O₃ production by multiplying the hourly value with a typical day length of 12 h, yielding a value of 2.4 ppbv/d (range: 1.62 – 4.77 ppbv/d). This is in good agreement with observations over the Brazilian rain forest during ABLE 2B (1.5 – 1.7 ppbv/d) for conditions with an inflow from rural areas (Pickering et al., 1992a). For storms with an inflow characterized by urban environments

10 generally higher values were deduced during ABLE 2B (16.5 – 17.2 ppbv/d) (Pickering et al., 1992a). Higher values were also observed for convective transport from biomass burning plumes during ABLE 2A over South America (7.4 – 8.5 ppbv/d) (Pickering et al., 1992b), while smaller values of the order of 1 – 1.5 ppbv/d have been observed over tropical oceans (Pickering et al., 1993; Schulz et al., 1999; Kita et al., 2003; Koike et al., 2007).

During HOOVER II an eastward moving mesoscale convective system developed over the southern part of Germany on July

15 19, 2007. During a research flight out of Baaden airport, in- and outflow of a strong convective cell were probed close to Dresden, the capital of the State of Saxony. The outflow at 10.5 km altitude showed enhancements relative to background mixing ratios for CO, NO, OH and HO₂ by 85%, 600%, 350% and 150%, respectively, due to almost undiluted transport of boundary layer air to the upper troposphere and strong lightning activity. Ozone in the outflow was 20% lower than in background air (Bozem et al., 2017). As shown in Figure 6b this leads to a median NOPR of 1.89 ppbv/h (mean: 1.9 ± 0.28

20 ppbv/h), a factor of 6 higher than the upper tropospheric background for HOOVER II (median: 0.29 ppbv/h; mean: 0.31 ± 0.07 ppbv/h). The NOPR in the case study over Europe is an order of magnitude larger than over South America during GABRIEL. Median mixing ratios for NO during HOOVER and GABRIEL were 0.96 ppbv and 0.1 ppbv, respectively. Thus the difference in NOPR for the two case studies is mainly due to different NO concentrations. The median daily net ozone production for the HOOVER case is 22.67 ppbv/d (range: 19.47 – 26.11 ppbv/d) and about a factor of 2 – 4 larger than

25 values reported in the literature for NH mid-latitudes, e.g. ~ 15 ppbv/d during PRESTORM, Oklahoma (Pickering et al., 1990; Pickering et al., 1992a), 10 – 13 ppbv/d during STERAO-A over North America (DeCaria et al., 2005), up to 5 ppbv during EULINOX over Europe (Ott et al., 2007), and 5 – 7 ppbv/d during DC3 over North America (Apel et al., 2015).

4. Discussion and conclusions

30 The net O₃ tendencies derived from both in-situ observations and 3D-model simulations confirm earlier studies with net O₃ formation (NOPR > 0) taking place in the continental boundary layer and the upper troposphere (above approx. 7 km in the tropics and mid-latitudes), and net O₃ destruction (NOPR < 0) in the marine boundary layer and the lower free troposphere (between 1 and 6 km altitude). The main reason that explains this distinction is shown to be the NO concentration. Both



observations and model simulations indicate that the fate of ozone depends on the amount of NO relative to the threshold NO concentration, derived from Eq. 7. In our study, the observed NO concentrations are always close to NO_{th} (between 10% and several 100%). The NOPR values are therefore almost linearly dependent on NO, being typical for NO_x limited O_3 production regimes (Seinfeld and Pandis, 1998).

5 This strong NO dependency also affects the comparison between in-situ observations and model simulations. Although NOPR values show similar tendencies, absolute values are often slightly different, with the modelled absolute NOPR values typically being smaller in magnitude than observed (both for production and destruction regimes). This is partly due to differences in measured and simulated NO concentrations, as has been discussed for HOOVER II. An additional factor influencing the comparison is the calculated threshold NO value, which often differs for the observations and model
10 simulations. This indicates that the reasons for the model-observation differences are complex and depend on more than one parameter.

One remarkable feature is the shift to positive NOPR values above approx. 7 km altitude that is found in both observations and simulations. This shift occurs, although NO_{th} shows a tendency to increase at the highest altitudes. According to Eq. 7 this increase in NO_{th} can be either due to an increase in the O_3 sinks (photolysis and subsequent reaction with H_2O or
15 reaction with OH or HO_2) or a decrease in the O_3 source (concentrations of HO_2 and CH_3O_2). Due to the pressure decrease by a factor of 4 from the surface to 10 km altitude the concentrations of the radical precursors (CO, CH_4) also decrease by a factor of 4 which strongly reduces the concentrations of HO_2 and CH_3O_2 radicals and thus the denominator of Eq. 7. Ozone exhibits strongly increasing mixing ratios with altitude that compensate the pressure reduction effect, leading to an almost constant concentration throughout the troposphere. Overall this leads to a rather invariable O_3 loss rate throughout the
20 troposphere and thus an increase of NO_{th} with altitude. To obtain net O_3 production above 7 km altitude, a strong increase in NO concentrations with altitude is required. This NO increase with altitude is partly due to a shift in the partitioning in NO_x , yielding higher NO concentrations at high altitude due to the temperature dependency of the $\text{NO} + \text{O}_3$ reaction, whose rate constant decreases with decreasing temperature (Ehhalt et al., 1992; Ziereis et al., 2000). Additional sources of NO associated with convection and lightning further enhance NO at high altitude (Schumann and Huntrieser, 2007), resulting in
25 the positive NOPR values above 7 km altitude obtained for all three campaigns. The case studies of enhanced NOPR values associated with convection and lightning produced NO_x in section 3.5 thus indicate that the general increase of NOPR above 7 km altitude is most likely due to the integral effect of convection on the upper troposphere.

Acknowledgements. The authors would like to thank Uwe Parchatka, Rainer Königstedt, and Corinne Schiller for their help
30 with the measurements. Also we would like to acknowledge the support from the GABRIEL and HOOVER teams, enviscope GmbH (Frankfurt), and GFD (Gesellschaft für Zielflugdarstellung, Hohn).



References

- Apel, E. C., R. S. Hornbrook, A. J. Hills, N. J. Blake, M. C. Barth, A. Weinheimer, C. Cantrell, S. A. Rutledge, B. Basarab, J. Crawford, G. Diskin, C. R. Homeyer, T. Campos, F. Flocke, A. Fried, D. R. Blake, W. Brune, I. Pollack, J. Peischl, T. Ryerson, P. O. Wennberg, J. D. Crouse, A. Wisthaler, T. Mikoviny, G. Huey, B. Heikes, D. O'Sullivan, and D. D. Riemer: Upper tropospheric ozone production from lightning NO_x-impacted convection: Smoke ingestion case study from the DC3 campaign. *J. Geophys. Res. Atmos.*, 120, 2505–2523. doi: 10.1002/2014JD022121, 2015.
- Bozem, H., Fischer, H., Gurk, C., Schiller, C. L., Parchatka, U., Koenigstedt, R., Stickler, A., Martinez, M., Harder, H., Kubistin, D., Williams, J., Eerdeken, G., and Lelieveld, J.: Influence of corona discharge on the ozone budget in the tropical free troposphere: a case study of deep convection during GABRIEL, *Atmos. Chem. Phys.*, 14, 8917–8931, doi:10.5194/acp-14-8917-2014, 2014.
- Bozem, H., Pozzer, A., Harder, H., Martinez, M., Williams, J., Lelieveld, J., and Fischer, H.: The influence of deep convection on HCHO and H₂O₂ in the upper troposphere over Europe, submitted to *Atmos. Chem. Phys.*, 2017.
- Cantrell, C. A., R. E. Shetter, T. M. Gilpin, and J. G. Calvert: Peroxy radicals measured during Mauna Loa Observatory Photochemistry Experiment 2: The data and first analysis, *J. Geophys. Res.*, 101, 14643–14652, doi:10.1029/95JD01698, 1996.
- Cantrell, C.A., et al.: Peroxy radical behaviour during the Transport and Chemical Evolution over the Pacific (TRACE-P) campaign as measured aboard the NASA P-3B aircraft, *J. Geophys. Res.*, 108, 8797, doi:10.1029/2003JD003674, 2003a.
- Cantrell, C.A., et al.: Steady state free radical budgets and ozone photochemistry during TOPSE, *J. Geophys. Res.*, 108, 8361, doi:10.1029/2002JD002198, 2003b.
- Cazorla, M. and Brune, W. H.: Measurement of Ozone Production Sensor, *Atmos. Meas. Tech.*, 3, 545–555, doi:10.5194/amt-3-545-2010, 2010.
- Colomb, A., J. Williams, J. Crowley, V. Gros, R. Hofmann, G. Salisbury, T. Kluepfel, R. Kormann, A. Stickler, C. Forster, J. Lelieveld: Airborne measurements of trace organic species in the upper troposphere over Europe: the impact of deep convection. *Environ. Chem.* 3, 244–259, doi:10.1071/EN06020, 2006.



- DeCaria, A. J., K. E. Pickering, G. L. Stenchikov, and L. E. Ott: Lightning-generated NO_x and its impact on tropospheric ozone production: A three-dimensional modeling study of a Stratosphere-Troposphere Experiment: Radiation, Aerosols and Ozone (STRAO-A) thunderstorm, *J. Geophys. Res.*, 110, D14303, doi:10.1029/2004JD005556, 2005
- 5 DiNunno, B., Davis, D., Chen, G., Crawford, J., Olson, J., and Liu, S.: An assessment of ozone photochemistry in the central/eastern North Pacific as determined from multiyear airborne field studies, *J. Geophys. Res.*, 108, 8237, doi:10.1029/2001JD001468, 2003.
- Ehhalt, D. H., F. Rohrer, and A. Wahner: Sources and distribution of NO_x in the upper troposphere at northern mid-latitudes, *J. Geophys. Res.*, 97, 3725–3738, doi:10.1029/91JD03081, 1992.
- 10 Fischer, H., Kormann, R., Klüpfel, T., Gurk, Ch., Königstedt, R., Parchatka, U., Mühle, J., Rhee, T. S., Brenninkmeijer, C. A. M., Bonasoni, P., and Stohl, A.: Ozone production and trace gas correlations during the June 2000 MINATROC intensive measurement campaign at Mt. Cimone, *Atmos. Chem. Phys.*, 3, 725–738, doi:10.5194/acp-3-725-2003, 2003.
- 15 Fischer, H., Lawrence, M., Gurk, Ch., Hoor, P., Lelieveld, J., Hegglin, M. I., Brunner, D., and Schiller, C.: Model simulations and aircraft measurements of vertical, seasonal and latitudinal O₃ and CO distributions over Europe, *Atmos. Chem. Phys.*, 6, 339–348, doi:10.5194/acp-6-339-2006, 2006.
- 20 Gurk, Ch., Fischer, H., Hoor, P., Lawrence, M. G., Lelieveld, J., and Wernli, H.: Airborne in-situ measurements of vertical, seasonal and latitudinal distributions of carbon dioxide over Europe, *Atmos. Chem. Phys.*, 8, 6395–6403, doi:10.5194/acp-8-6395-2008, 2008.
- Hosaynali Beygi, Z., Fischer, H., Harder, H. D., Martinez, M., Sander, R., Williams, J., Brookes, D. M., Monks, P. S., and
25 Lelieveld, J.: Oxidation photochemistry in the Southern Atlantic boundary layer: unexpected deviations of photochemical steady state, *Atmos. Chem. Phys.*, 11, 8497–8513, doi:10.5194/acp-11-8497-2011, 2011.
- Junge, C.E.: Air chemistry and radioactivity, International Geophysics Series, New York, Academic Press, doi:
10.1002/qj.49709038422, 1963.
- 30 Haagen-Smith, A.J., and Fox, M.M.: *Ind. Eng. Chem.*, 48 (9), 1484–1487, doi: 10.1021/ie51400a033, 1956.



- Kanaya, Y., Matsumoto, J., and Akimoto, H.: Photochemical ozone production at a subtropical island of Okinawa, Japan: Implications from simultaneous observations of HO₂ radical and NO_x, *J. Geophys. Res.*, 107, 4368, doi:10.1029/2001JD000858, 2002.
- 5 Kita, K., et al.: Photochemical production of ozone in the upper troposphere in association with cumulus convection over Indonesia, *J. Geophys. Res.*, 108, 8400, doi:10.1029/2001JD000844, 2003.
- Kleinman, L.I.: Ozone process insights from field experiments – part II: Observation-based analysis for ozone production, *Atmos. Environ.*, 34, 2023-2033, doi:10.1016/S1352-2310(99)00457-4, 2000.
- 10 Kleinman, L.I., Daum, P.H., Lee, Y.-N., Nunnermacker, L.J., Sprinston, S.R., Weinstein-Lloyd, J., and Rudolph, J.: A comparative study of ozone production from five U.S. metropolitan areas, *J. Geophys. Res.*, 110, D02301, doi:10.1029/2004JD005096, 2005.
- 15 Klippel, T., Fischer, H., Bozem, H., Lawrence, M. G., Butler, T., Jöckel, P., Tost, H., Martinez, M., Harder, H., Regelin, E., Sander, R., Schiller, C. L., Stickler, A., and Lelieveld, J.: Distribution of hydrogen peroxide and formaldehyde over Central Europe during the HOOVER project, *Atmos. Chem. Phys.*, 11, 4391-4410, doi:10.5194/acp-11-4391-2011, 2011.
- 20 Klonecki, A. and Levy, H.: Tropospheric chemical ozone tendencies in CO-CH₄-NO_y-H₂O system: Their sensitivity to variations in environmental parameters and their application to a global chemistry transport model study. *J. Geophys. Res.*, 102, 21221-21237, doi: 10.1029/97JD01805, 1997.
- Ko, M., Hu, W., Rodriguez, J.M., Kondo, Y., Koike, M., Kita, K., Kawakami, S., Blake, D., Liu, S., and Ogawa, T.: Photochemical ozone budget during the BIBLE A and B campaigns, *J. Geophys. Res.*, 108, 8404, doi:10.1029/2001JD000800, 2003.
- 25 Koike, M., et al.: Measurements of reactive nitrogen produced by tropical thunderstorms during BIBLE-C, *J. Geophys. Res.*, 112, D18304, doi:10.1029/2006JD008193, 2007.
- 30 Kondo, Y., et al.: Photochemistry of ozone over the western Pacific from winter to spring, *J. Geophys. Res.*, 109, D23S02, doi: 10.1029/2004JD004871, 2004.
- Kubistin, D., Harder, H., Martinez, M., Rudolf, M., Sander, R., Bozem, H., Eerdekens, G., Fischer, H., Gurk, C., Klupfel, T., Konigstedt, R., Parchatka, U., Schiller, C. L., Stickler, A., Taraborrelli, D., Williams, J., and Lelieveld, J.: Hydroxyl radicals



- in the tropical troposphere over the Suriname rainforest: comparison of measurements with the box model MECCA, *Atmos Chem Phys*, 10, 9705-9728, 10.5194/acp-10-9705-2010, 2010.
- 5 Kuhn, U., et al.: Impact of Manaus City on the Amazon Green Ocean atmosphere: ozone production, precursor sensitivity and aerosol load, *Atmos. Chem. Phys.*, 10, 9251-9282, doi: 10.5194/acp-10-9251-2010, 2010.
- Lawrence, M. G., Rasch, P. J., von Kuhlmann, R., Williams, J., Fischer, H., de Reus, M., Lelieveld, J., Crutzen, P. J., Schultz, M., Stier, P., Huntrieser, H., Heland, J., Stohl, A., Forster, C., Elbern, H., Jakobs, H., and Dickerson, R. R.: Global chemical weather forecasts for field campaign planning: predictions and observations of large-scale features during MINOS, CONTRACE, and INDOEX, *Atmos. Chem. Phys.*, 3, 267-289, doi:10.5194/acp-3-267-2003, 2003.
- 10 Leighton, P.A.: Photochemistry of air pollution, Academic Press, New York, 1961.
- Lelieveld, J., and Dentener, F. J.: What controls tropospheric ozone?, *J. Geophys. Res.*, 105(D3), 3531–3551, doi:10.1029/1999JD901011, 2000.
- 15 Lelieveld, J. Butler, T.M., Crowley, J.N., Dillon, T.J., Fischer, H., Ganzeveld, L., Harder, H., Lawrence, M.G., Martinez, M., Taraborrelli, D., and Williams, J.: Atmospheric oxidation capacity sustained by a tropical forest, *Nature*, 452, 737-740, doi:10.1038/nature06870, 2008.
- 20 Liu, Z. et al.; Summertime photochemistry during CAREBeijing-2007: RO_x budgets and O₃ formation, *Atmos Chem. Phys.*, 12, 7737-7752, doi: 10.5194/acp-12-7737-2012, 2012.
- Madronich, S., and Flocke, S.: The role of solar radiation in atmospheric chemistry, in *The Handbook of Environmental Chemistry Vol.2 Part L Environmental Photochemistry* (ed. By P. Boule), Springer, Berlin, 1999.
- 25 Martinez, M., Harder, H., Kubistin, D., Rudolf, M., Bozem, H., Eerdekens, G., Fischer, H., Klüpfel, T., Gurk, C., Königstedt, R., Parchatka, U., Schiller, C. L., Stickler, A., Williams, J., and Lelieveld, J.: Hydroxyl radicals in the tropical troposphere over the Suriname rainforest: airborne measurements, *Atmos. Chem. Phys.*, 10, 3759-3773, doi:10.5194/acp-10-3759-2010, 2010.
- 30 Olivier, J.G.J., Peters, J.A.H.W., Bakker, J., Berdowski, J.J.M., Visschedijk, A.J.H., and Bloos, J.P.J.: Applications of EDGAR: Emission data base for atmospheric research, Rep. 410.200.051.RIVM, RIVM, Bilthoven, The Netherlands, 2002.



- Ott, L. E., K. E. Pickering, G. L. Stenchikov, H. Huntrieser, and U. Schumann: Effects of lightning NO_x production during the 21 July European Lightning Nitrogen Oxides Project storm studied with a three-dimensional cloud-scale chemical transport model, *J. Geophys. Res.*, 112, D05307, doi:10.1029/2006JD007365, 2007.
- 5 Penkett, S. A., P. S. Monks, L. J. Carpenter, K. C. Clemitshaw, G. P. Ayers, R. W. Gillett, I. E. Galbally, and C. P. Meyer: Relationships between ozone photolysis rates and peroxy radical concentrations in clean marine air over the Southern Ocean, *J. Geophys. Res.*, 102, 12805–12817, doi:10.1029/97JD00765, 1997.
- Pickering, K. E., A. M. Thompson, R. R. Dickerson, W. T. Luke, D. P. McNamara, J. P. Greenberg, and P. R. Zimmerman:
10 Model calculations of tropospheric ozone production potential following observed convective events, *J. Geophys. Res.*, 95, 14049–14062, doi:10.1029/JD095iD09p14049, 1990.
- Pickering, K. E., A. M. Thompson, J. R. Scala, W.-K. Tao, R. R. Dickerson, and J. Simpson: Free tropospheric ozone
15 production following entrainment of urban plumes into deep convection, *J. Geophys. Res.*, 97, 17985–18000, doi:10.1029/92JD01716, 1992a.
- Pickering, K.E., Thompson, A.M., Scala, J.R., Tao, W.K., and Simpson, J.: Ozone production potential following convective redistribution of biomass burning emissions, *J. Atmos. Chem.*, 14, 297–313, doi:10.1007/BF00115241, 1992b.
- 20 Pickering, K. E., A. M. Thompson, W.-K. Tao, and T. L. Kucsera: Upper tropospheric ozone production following mesoscale convection during STEP/EMEX, *J. Geophys. Res.*, 98, 8737–8749, doi:10.1029/93JD00875, 1993.
- Reeves, C.E., Penkett, S., Bauguitte, S., Law, K.S. Evans, M.J., Bandy, B.J., Monks, P.S., Edwards, G.D., Phillips, G.,
25 Barjat, H., Kent, J., Dewey, K., Schmitgen, S., and Kley, D.: Potential for photochemical ozone formation in the troposphere over the North Atlantic as derived from aircraft observations during ASCOE, *J. Geophys. Res.*, 107, 4707, doi:10.1029/2002JD002415, 2002.
- Regelin, E., Harder, H., Martinez, M., Kubistin, D., Tatum Ernest, C., Bozem, H., Klippel, T., Hosaynali-Beygi, Z., Fischer, H., Sander, R., Jöckel, P., Königstedt, R., and Lelieveld, J.: HO_x measurements in the summertime upper troposphere over
30 Europe: a comparison of observations to a box model and a 3-D model, *Atmos. Chem. Phys.*, 13, 10703–10720, doi:10.5194/acp-13-10703-2013, 2013.
- Ren, X., et al.: Atmospheric oxidation chemistry and ozone production: Results from SHARP 2009 in Houston, Texas, *J. Geophys. Res. Atmos.*, 118, 5770–5780, doi:10.1002/jgrd.50342, 2013.



- Roelofs, G.-J. and Lelieveld, J.: Model study of the influence of cross-tropopause O₃ transports on tropospheric O₃ levels. *Tellus B*, 49: 38–55, doi: 10.1034/j.1600-0889.49.issue1.3.x, 1997.
- 5 Seinfeld, J.H., and Pandis, S.N.: *Atmospheric Chemistry and Physics*, pp. 299-302, John Wiley & Sons, New York, USA, 1998.
- Schiller, C.I., Bozem, H., Gurk, C., Parchatka, U., Königstedt, R., Harris, G.W., Lelieveld, J., and Fischer, H.: Applications of quantum cascade lasers for sensitive trace gas measurements of CO, CH₄, N₂O, and HCHO, *Appl. Phys.*, B92, 419-430, doi:10.1007/s00340-008-3125-0, 2008.
- 10 Schultz, M. G., et al.: On the origin of tropospheric ozone and NO_x over the tropical South Pacific, *J. Geophys. Res.*, 104, 5829–5843, doi:10.1029/98JD02309, 1999.
- 15 Schumann, U. and Huntrieser, H.: The global lightning-induced nitrogen oxides source, *Atmos. Chem. Phys.*, 7, 3823-3907, doi:10.5194/acp-7-3823-2007, 2007.
- Sommariva, R., et al.: Ozone production in remote oceanic and industrial areas derived from ship based measurements of peroxy radicals during TexAQS 2006: *Atmos. Chem. Phys.*, 11, 2471-2485, doi: 10.5194/acp-11-2471-2011, 2011.
- 20 Stickler, A., H. Fischer, J. Williams, M. de Reus, R. Sander, M. G. Lawrence, J. N. Crowley, and J. Lelieveld: Influence of summertime deep convection on formaldehyde in the middle and upper troposphere over Europe, *J. Geophys. Res.*, 111, D14308, doi:10.1029/2005JD007001, 2006.
- 25 Taraborrelli, D., M.G. Lawrence, J.N. Crowley, T.J. Dillon, S. Gromov, C.B.M. Groß, L. Vereecken, and J. Lelieveld: Hydroxyl radical buffered by isoprene oxidation over tropical forests, *Nature Geosci.*, 5, 190-193, doi:10.1038/ngeo1405, 2012.
- von Kuhlmann, R., M. G. Lawrence, P. J. Crutzen, and P. J. Rasch: A model for studies of tropospheric ozone and nonmethane hydrocarbons: Model evaluation of ozone-related species, *J. Geophys. Res.*, 108, 4729, doi:10.1029/2002JD003348, 2003.
- 30



- Zanis, P., P. S. Monks, E. Schuepbach, L. J. Carpenter, T. J. Green, G. P. Mills, S. Bauguitte, and S. A. Penkett: In situ ozone production under free tropospheric conditions during FREETEX '98 in the Swiss Alps, *J. Geophys. Res.*, 105, 24223–24234, doi:10.1029/2000JD900229, 2000.
- 5 Zierys, H., H. Schlager, P. Schulte, P. F. J. vanVelthoven, and F. Slemr: Distributions of NO, NO_x, and NO_y in the upper troposphere and lower stratosphere between 28° and 61°N during POLINAT 2, *J. Geophys. Res.*, 105, 3653–3664, doi:10.1029/1999JD900870, 2000.



Table 1: Precision, accuracy and detection limit of the in-situ measurements used to deduce NOPR

	<i>Precision (1σ)</i>	<i>Accuracy</i>	<i>Detection limit</i>
$J(NO_2)$	1%	10%	
CO	< 1 %	1 %	
CH_4	< 1 %	1 %	
H_2O		5 %	200 ppmv
O_3	4 %	2 %	2 ppbv
NO	7 %	12 %	5 pptv
OH	7 %	18 %	0.02 pptv
HO_2	1 %	18 %	0.07 pptv

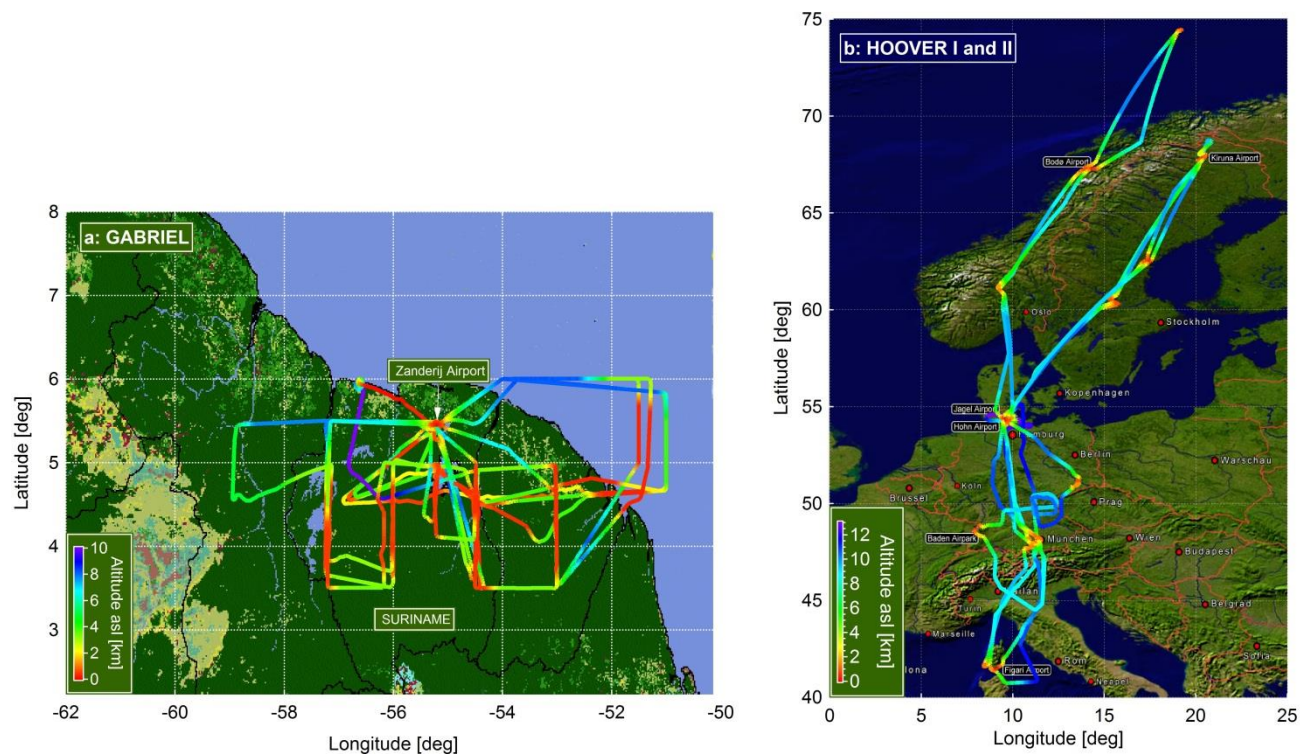


Figure 1: Flight tracks during GABRIEL (a: left panel) and HOOVER I and II (b: right panel).

5

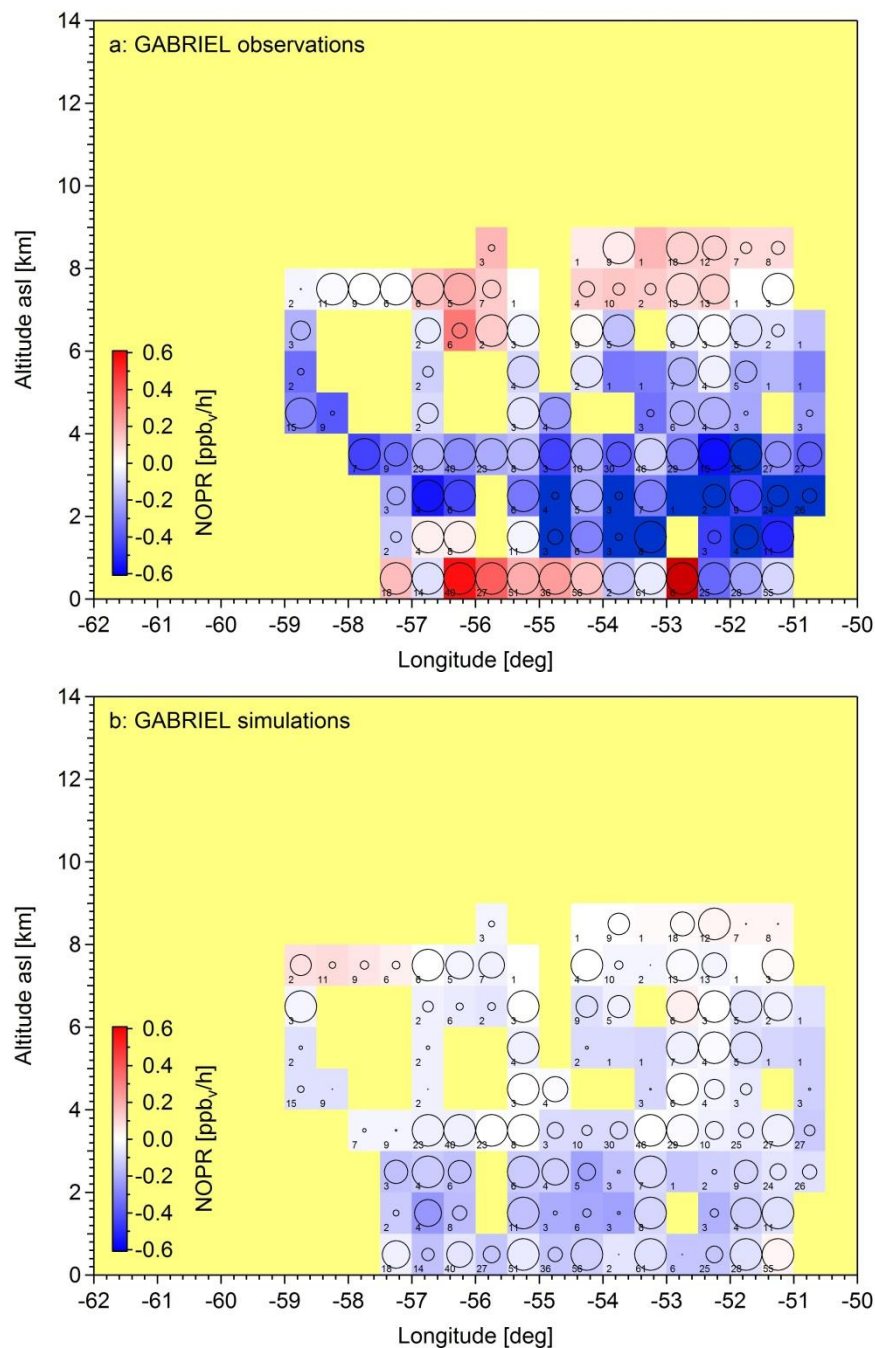


Figure 2: Net ozone production rates (NOPR) in ppbv/h calculated from in-situ data (a: upper panel) and from MATCH
5 simulations (b: lower panel) for GABRIEL.

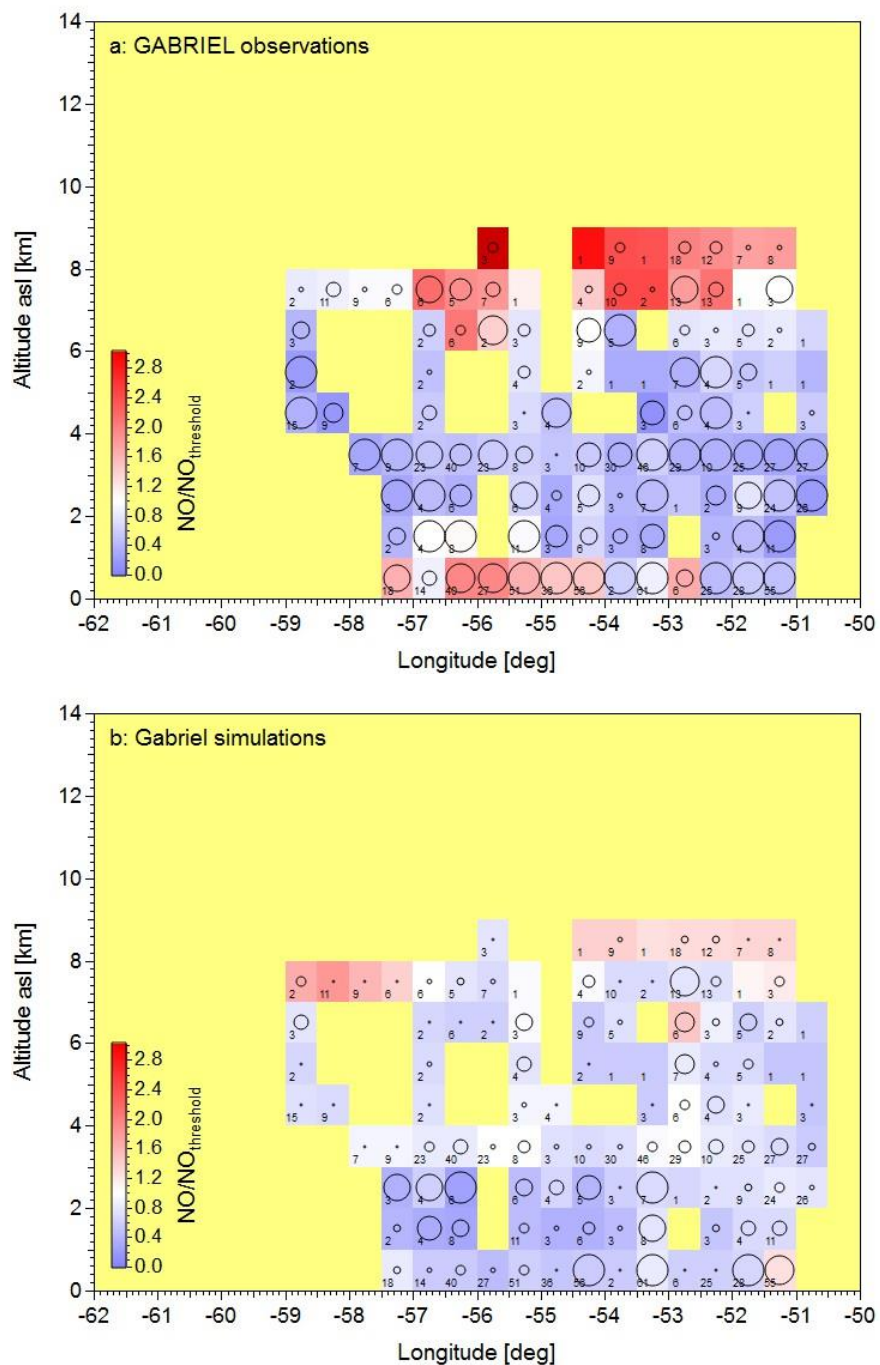


Figure 3: Ratio of NO to NO_{th} deduced from in-situ data (a: upper panel) and MATCH simulations (b: lower panel) for GABRIEL.

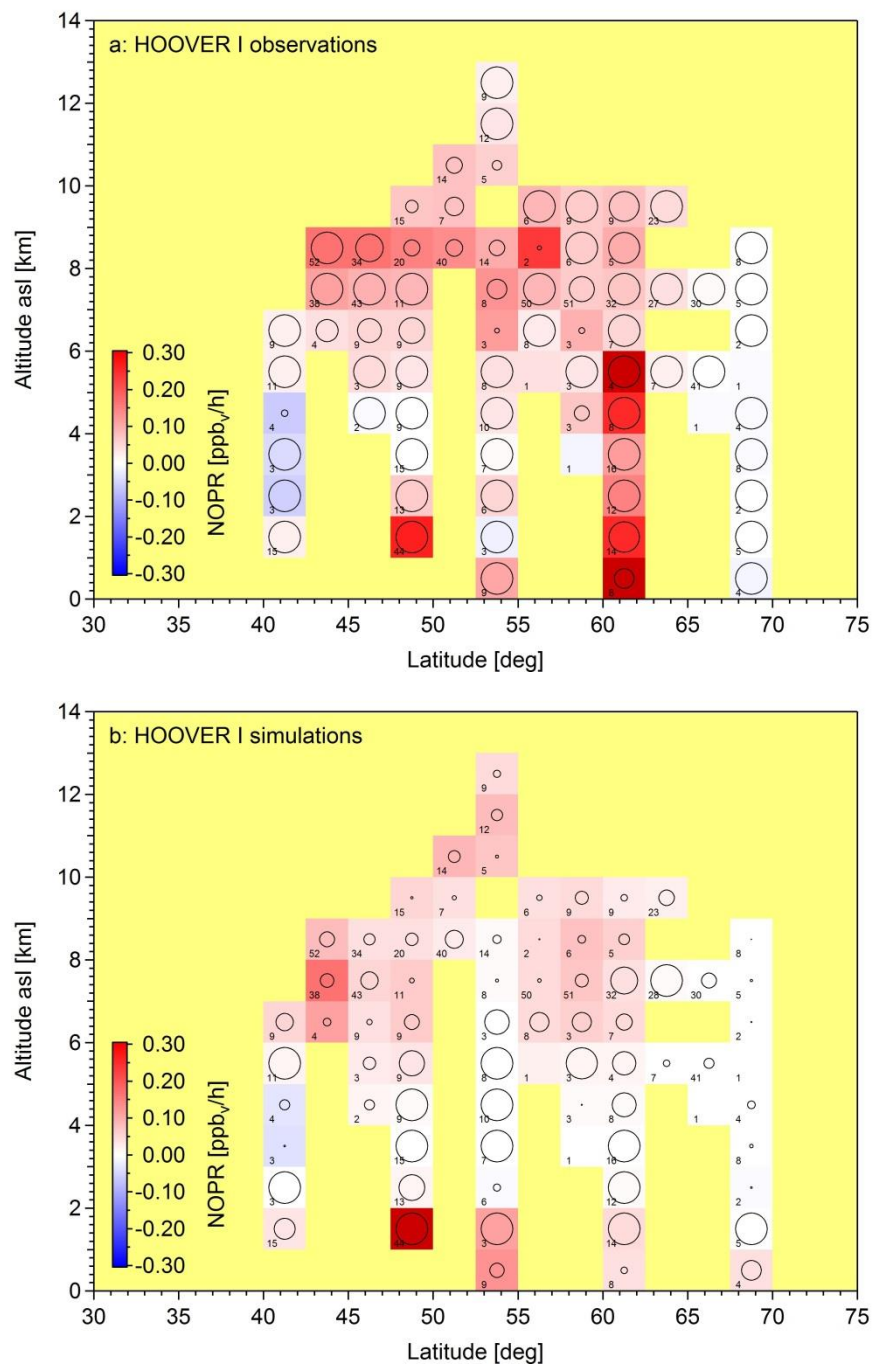
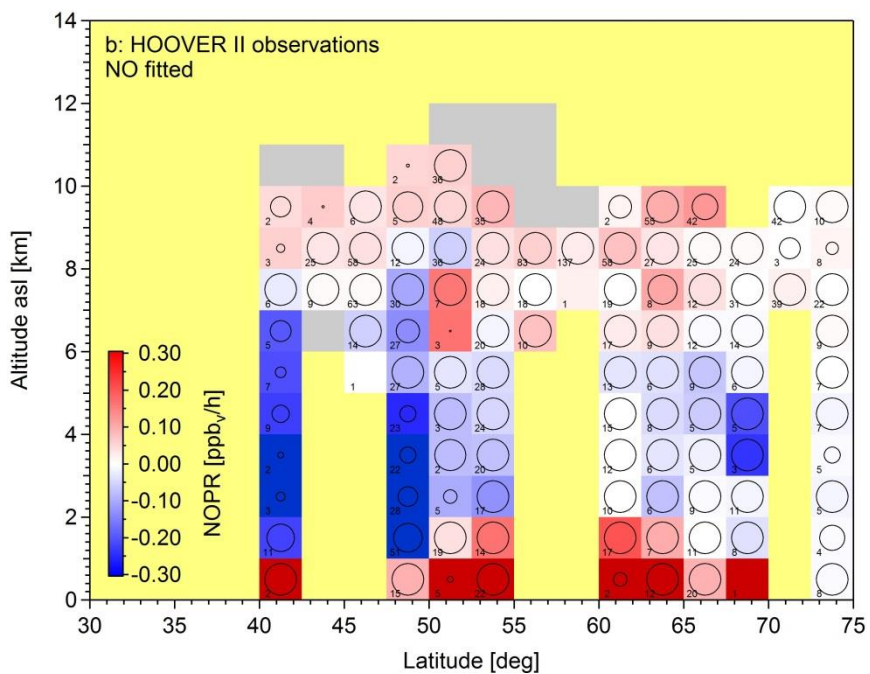
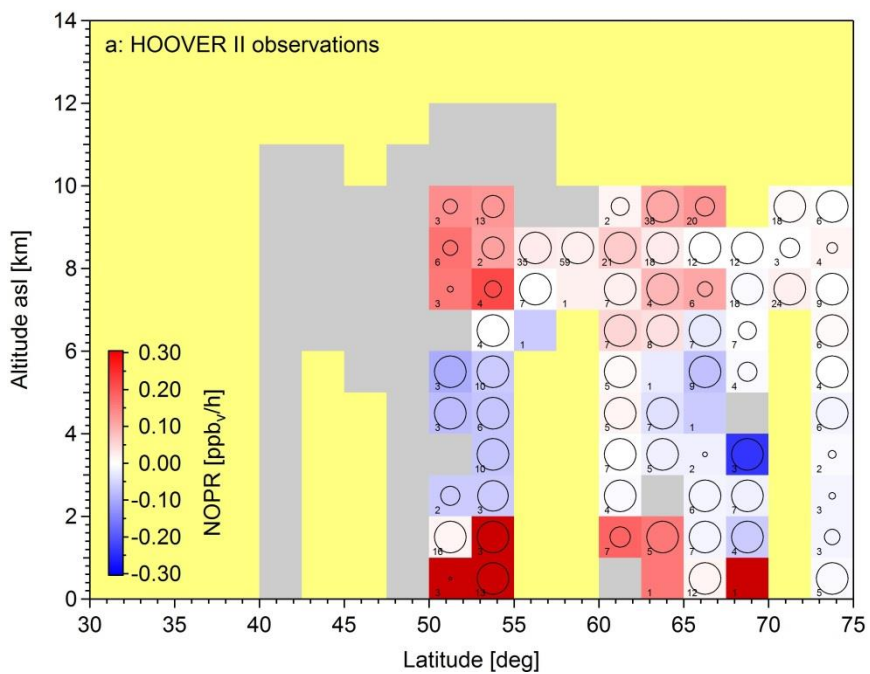


Figure 4: Net ozone production rates (NOPR) in ppbv/h calculated from in-situ data (a: upper panel) and from MATCH
5 simulations (b: lower panel) for HOOVER I.



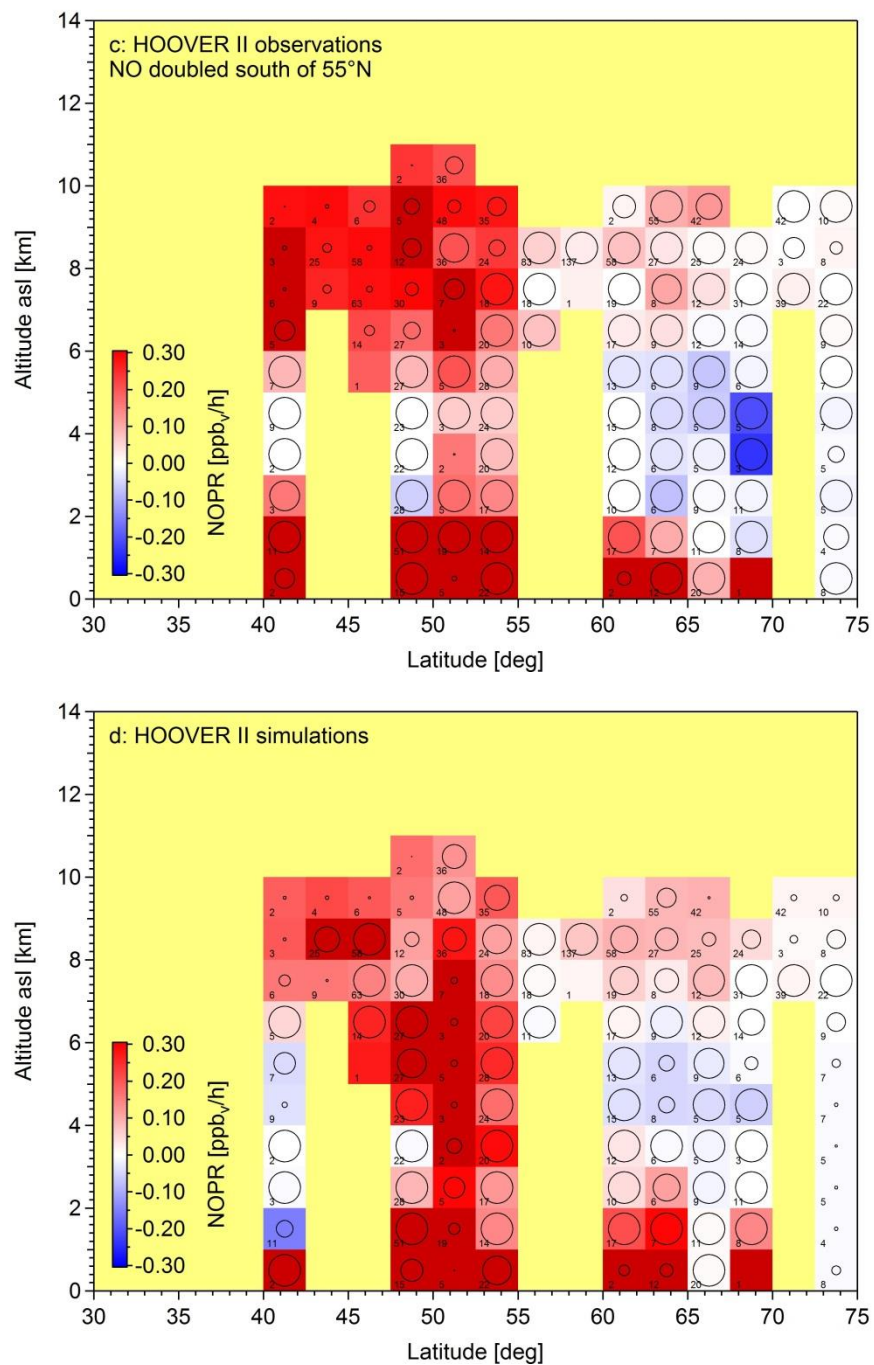


Figure 5: Net ozone production rates (NOPR) in ppbv/h calculated from in-situ data (a), fitted NO (b), double NO (c) and from MATCH simulations (b) for HOOVER II.

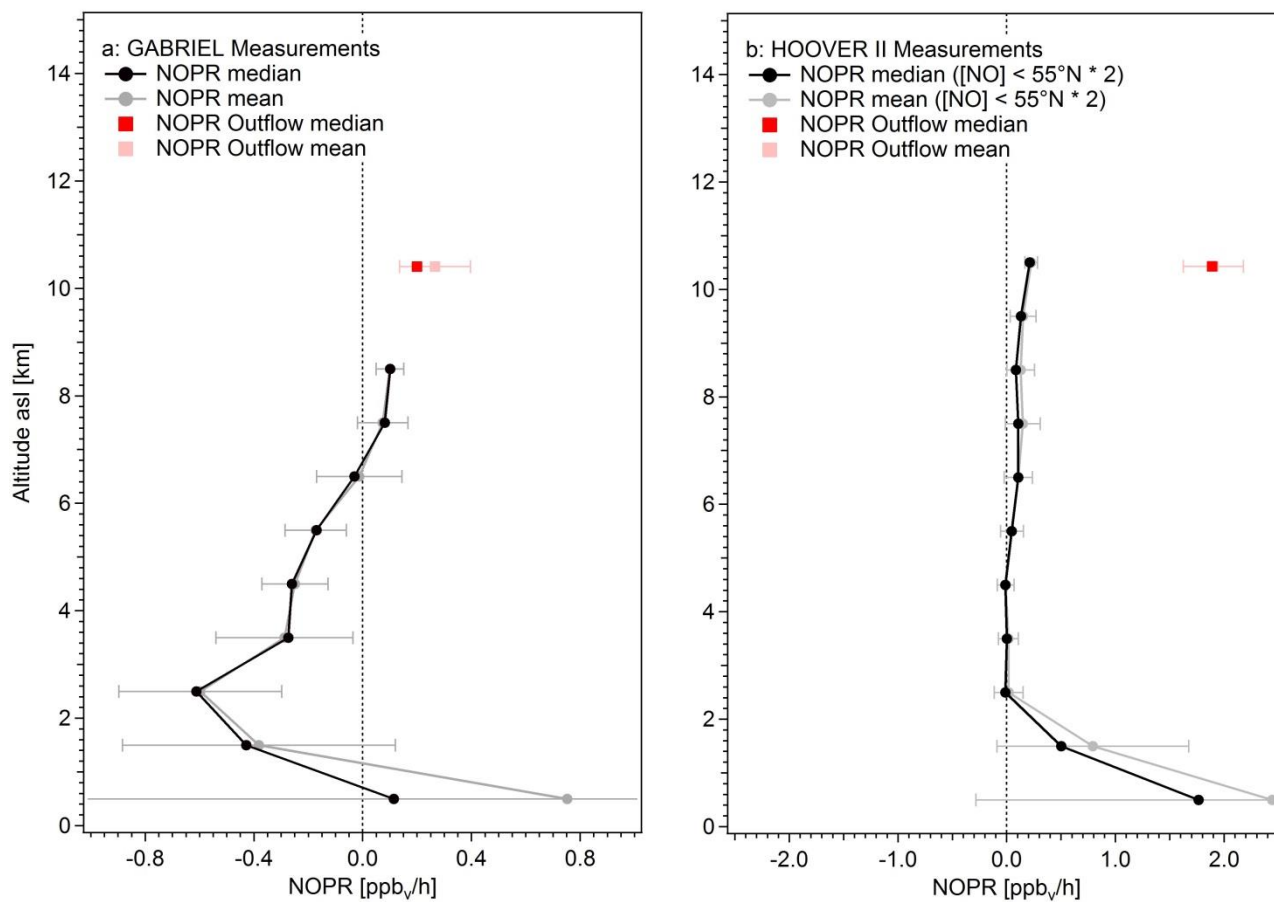


Figure 6: Net ozone production rates (NOPR) in ppbv/h (red squares) calculated from in-situ data for convective events during GABRIEL (a: left panel) and HOOVER II (b: right panel) relative to campaign average profiles (black).